Applied Catalysis B: Environmental 207 (2017) 385–396

Contents lists available at ScienceDirect

Applied Catalysis B: Environmental

journal homepage: www.elsevier.com/locate/apcatb

Redox-performance correlations in Ag–Cu–Mg–Al, Ce–Cu–Mg–Al, and Ga–Cu–Mg–Al hydrotalcite derived mixed metal oxides

Magdalena Jabłońska [a], Katja Nothdurft [a], Marek Nocuń [b], Vladimir Girman [c], Regina Palkovits [a,*]

[a] Institut für Technische und Makromolekulare Chemie, Chair of Heterogeneous Catalysis and Chemical Technology, RWTH Aachen University, Worringerweg 2, 52074 Aachen, Germany
[b] Faculty of Material Science and Ceramics, AGH University of Science and Technology, Mickiewicza 30, 30-059 Kraków, Poland
[c] Department of Condensed Matter Physics, Pavol Jozef Šafárik University in Košice, Park Angelinum 9, 041 54 Košice, Slovakia

ARTICLE INFO

Article history:
Received 31 October 2016
Received in revised form 9 January 2017
Accepted 28 January 2017
Available online 1 February 2017

Keywords:
Hydrotalcite-like compounds
Mixed metal oxides
Copper
Ammonia oxidation

ABSTRACT

Ag-, Ce- and Ga-promoted Cu–Mg–Al hydrotalcite derived mixed metal oxides were obtained by standard coprecipitation, followed by calcination. The obtained Ag(Ce, Ga)–Cu–Mg–Al–O_x mixed metal oxides were characterized with respect to their crystalline structure (XRD, TEM), texture (BET), surface acidity (NH_3-TPD), redox properties (H_2-TPR), chemical surface composition (XPS), and tested in the selective catalytic oxidation of ammonia into nitrogen and water vapour (NH_3-SCO). The loading of Ag_y-, Ce_y-, or Ga_y–Cu_5–Mg_{66-y}–Al_{29} ($y = 0$–1) had a clear effect on the catalytic performances. For materials with low metal loadings ($y \leq 0.25$), the redox properties determined the catalytic performances in NH_3-SCO. The formation of easily reducible CuO_x played a crucial role for enhanced catalytic activity at lower temperatures, with a drop in the selectivity to N_2 at higher temperatures. Higher metal loading ($y \geq 0.5$) led to the formation of surface and bulk copper oxide species, and other aggregated metal oxide phases, which enhanced the catalytic activity for Ag–Cu–Mg–Al–O_x, and diminished activity for Ce(Ga)–Cu–Mg–Al–O_x.

1. Introduction

Hydrotalcite-like compounds can be represented by the general formula $M^{2+}{}_{1-y}\ M^{3+}{}_y\ (OH)_2\ (A^{n-})_{y/n} \cdot mH_2O$, where M^{2+} and M^{3+} are bi- and trivalent metal cations, respectively. A^{n-} presents an interlayer anion, and $y = M^{3+}/(M^{3+} + M^{2+})$ exhibits a value between 0.17 and 0.50 [1,2]. Thus, a great variety of possible metal combinations – including monovalent M^+ (e.g. Ag^+ or Li^+ [e.g. [3,4]]) or even tetravalent M^{4+} (e.g. Zr^{4+} or Sn^{4+} [e.g. [5,6]]) – led to a large number of possible materials. Hydrotalcite-like compounds serve mostly as precursors for mixed metal oxides with a high specific surface area, homogenous dispersion of metals within the oxide matrix, high thermal stability, etc. [7,8]. Among them, copper-containing hydrotalcite derived mixed metal oxides (Cu–Mg–Al–O_x, 5.0–8.0:66.0–63.0:29.0, mol.%) present the most active, selective to N_2 and stable catalysts among copper modified clays for the selective ammonia oxidation into nitrogen and water vapour (NH_3-SCO) [9,10]. On the other side, bi- or trimetallic (transition metal-copper) hydrotalcite derived mixed metal oxide systems, such as Pt(Pd,Rh)-Cu [11,12], Zn–Cu, Fe–Zn–Cu or Fe–Cu [7,13] were scarcely investigated in NH_3-SCO. However, the available studies revealed a correlation between the reduction temperature of CuO_x and the catalytic performance in ammonia oxidation. The proximity of other transition metals in Cu-based catalysts significantly influenced the reducibility of copper oxide species. Catalysts containing easily reducible CuO_x revealed enhanced activity together with a drop in N_2 selectivity at higher temperatures.

According to the literature [e.g. [9,11,14]], a cooperative effect of copper with other metals (e.g. noble metal, rare earth metal, etc.) clearly influences the reduction temperature of copper oxide species. Ag-, Ce-, or Ga-promoters should influence the reducibility of CuO_x over a broad range, and thus the catalytic performance in NH_3-SCO. However, a limited number of reports refer to bimetallic: Ag–Cu, Ce–Cu or Ga–Cu hydrotalcite derived mixed metal oxides. Recently, Xu et al. [15] reported Ag–Cu supported on Mg–Al–O_x for the dehydrogenative cross-coupling of primary and secondary benzylic alcohols. These catalysts were obtained through calcination and subsequent reduction in H_2; thus, both metals existed in the metallic form (based on XPS studies). For Ag–Cu deposited on inorganic supports (e.g. $BaCO_3$ [16], SiO_2 [17], or Al_2O_3 [18,19]), an enhanced CuO_x reducibility correlated with a distinct interaction between Ag and Cu species. One of the possible explanations refers to electronic interactions – copper reduction-silver oxida-

* Corresponding author.
E-mail address: Palkovits@itmc.rwth-aachen.de (R. Palkovits).

http://dx.doi.org/10.1016/j.apcatb.2017.01.079
0926-3373/

tion – in bimetallic Ag–Cu systems, together with an improved dispersion of CuO_x [e.g. [17,18]]. Analogously, cerium promoted the reduction of copper oxide species. Wang et al. [20] and Wen et al. [21] investigated Ce–Cu–Mg–Al–O_x for soot oxidation and NO reduction with CO, respectively. The presence of cerium enhanced the reduction of copper oxide species (based on H_2-TPR studies) [14], possibly due to the generation of a large quantity of easily reducible Cu^+ (based on XPS analysis) [21]. Although, Cu–Mg–Al hydrotalcite derived mixed oxides obtained through calcination in air only revealed the presence of Cu^{2+} species [e.g. [22,23]]. Cu^{2+}/Cu^+ coexisted also in CuO-CeO_2 mixed oxides prepared by a surfactant-templated method [24]. Gallium has mostly been studied in Mg–(Al)–Ga hydrotalcite derived systems [e.g. [25–28]], while only few reports refer to Cu–Ga catalysts [e.g. [29,30]]. For example, Venugopal et al. [29] investigated Ga–Cu–Zn–Al–O_x among (Y, Zr, La, Ga)–Cu–Zn–Al hydrotalcite derived mixed metal oxides for dimethyl ether synthesis. Gallium-containing samples reached the highest reduction temperature, indicating the presence of bulk CuO_x (based on H_2-TPR and SEM analysis). Moreover, the presence of gallium retarded the reduction of CuO_x in other Ga–Cu catalytic systems (e.g. CuO/Ga_2O_3–ZnO [31], CuO/Ga_2O_3 or CuO/Ga_2O_3–ZrO_2 [32], etc.). Thus, the presence of gallium led to the formation of bulk copper oxides species in the form of CuO_x and/or a $CuGa_2O_4$ spinel phase [32,33].

In the present work, we prepared hydrotalcite-like precursors of different composition by coprecipitation covering Ag_y-, Ce_y-, or Ga_y–Cu_5–Mg_{66-y}–Al_{29} (y = 0–1). We characterized the as-synthesized materials and/or their derived forms using XRD, TG–DTG, BET, NH_3-TPD, TEM, XPS and H_2-TPR, and tested them as catalysts in the selective ammonia oxidation. To the best of our knowledge, this study presents for the first time the redox-performance correlation of Ag–Cu, Ce–Cu, and Ga–Cu hydrotalcite derived mixed metal oxides for NH_3-SCO. Our aim was to gain a comprehensive understanding of the influence of different dopants (Ag, Ce or Ga) on CuO_x reducibility, and consequently on catalytic activity and selectivity in ammonia oxidation.

2. Experimental

2.1. Catalysts preparation

A series of hydrotalcite-like compounds with an intended composition of Y–Cu–Mg–Al (Y = Ag, Ga, Ce; y:5:66-y:29 (y = 0, 0.1, 0.25, 0.5, 0.75, 1)) were prepared by coprecipitation using 1 M aqueous solutions of the following metal nitrates: $Cu(NO_3)_2{\cdot}3H_2O$ (Sigma), $Mg(NO_3)_2{\cdot}6H_2O$ (Sigma), $Al(NO_3)_3{\cdot}9H_2O$ (Sigma), $AgNO_3$ (Sigma), $Ga(NO_3)_3$ (Chempur), $Ce(NO_3)_3{\cdot}6H_2O$ (Sigma). A solution of 1 M sodium hydroxide (Chemsolute) was used as precipitating agent. The solution of metal salts was dropped simultaneously with NaOH to a vigorously stirred aqueous solution at 60 °C containing a slightly over-stoichiometric excess of Na_2CO_3 (Sigma). The pH of the reaction mixture was maintained constant at 10.0 ± 0.2 throughout the whole synthesis. The obtained suspension was aged at 60 °C for another 0.5 h after complete coprecipitation. The solid was filtered, washed carefully with distilled water and dried at room temperature. Afterwards, all samples were crushed and calcined at 600 °C for 6 h with a heating ramp of 10 K/min, and in static air. The mixed metal oxides obtained from hydrotalcite-like compounds were kept in a desiccator in order to avoid the reconstruction of the hydroxide-like structure. For catalytic experiments, a fraction of particle size in the range of 0.250–0.500 mm was used.

2.2. Catalysts characterization

The X-ray diffraction analysis (XRD) of the as-synthesized hydrotalcite-like compounds and their calcined forms was performed applying a Siemens D5000 XRD diffractometer using Cu-Kα radiation (λ = 1.54056 Å, 45 kV, 40 mA). The cell parameters were calculated using a position of (1 1 0) reflection: $a = 2(d_{110})$ and positions of basal reflections: $c = [3(d_{003}) + 6(d_{006})]/2$. The crystal sizes were calculated from the Scherrer equation $D = 0.89{\cdot}\lambda/\beta{\cdot}\cos\theta$, where D is the crystallite size, λ is the X-ray wavelength, β is the line broadening and θ is the Bragg angle.

The thermogravimetric analysis (TG) of the hydrotalcite-like compounds (~20 mg) was carried out using a Netzsch STA 409C/CD operated under a flow of air (10 cm^3/min) in the temperature range of 30–1000 °C with a linear heating rate of 5 K/min.

The chemical composition of the samples was determined by ICP-MS using an Agilent Technologies 8800 Triple Quad spectrometer.

The specific surface area (S_{BET}) of the mixed metal oxides was determined by low-temperature (−196 °C) N_2 sorption using a Quantachrome Quadrasorb SI. Prior to nitrogen adsorption the samples were outgassed at 250 °C for 12 h using a Quantachrome Flovac degasser. The specific surface area (S_{BET}) was calculated using the Brunauer–Emmett–Teller (BET) multiple point method in the p/p_0 range from 0.05 to 0.3. Pore size distributions were obtained from analysis of the desorption branches of the nitrogen isotherms using the Barrett–Joyner–Halenda method.

The surface acidity of the mixed metal oxides was determined by temperature-programmed desorption of ammonia (NH_3-TPD) in a fixed-bed flow microreactor system equipped with a QMS MKS, Cirrus 2 detector. Prior to the analysis, the sample (100 mg) was outgassed in a flow of pure argon at 500 °C for 1 h, and afterwards cooled down to 70 °C. Subsequently, the sample was saturated with ammonia in a flow of 1.0 vol.% NH_3/Ar (20 cm^3/min) for about 2 h. Afterwards, the sample was purged with pure argon (about 2 h) in order to remove physisorbed ammonia. Finally, the desorption of ammonia was measured in the temperature range of 70–500 °C with a linear heating rate of 5 K/min in a flow of pure argon (20 cm^3/min).

The micrographs of selected mixed metal oxides were obtained using a transmission electron microscope JEOL 2100F working at 200 KV, with Field Emission Gun (FEG), EDX analysis and STEM detectors for bright and dark mode.

The redox properties of the mixed metal oxides were studied by temperature-programmed reduction (H_2-TPR) using the Quantachrome ChemBET Pulsar TPR/TPD. H_2-TPR runs for the samples (30 mg) were carried out starting from room temperature to 1000 °C, with a linear heating rate of 10 K/min and in a flow (25 cm^3/min) of 5.0 vol.% H_2/Ar. Water vapour was removed from effluent gas by means of a cold trap placed in an ice-water bath. The H_2 consumption was detected and recorded by a TCD detector.

The X-ray photoelectron spectra (XPS) of selected mixed metal oxides were measured on a VSW spectrometer equipped with a hemispherical analyzer. The photoelectron spectra were measured using a magnesium Mg Kα source (E = 1253.6 eV). The base pressure in the analysis chamber during the measurements was 3×10^{-6} Pa and the spectra were calibrated on a main carbon C 1s peak at 284.6 eV. The composition and chemical surrounding of the sample surface were investigated based on the areas and binding energies of Ag 3d, Ce 3d, Ga 3d, Cu 2p, Mg 2p, Al 2p, C 1s and O 1s photoelectron peaks. Mathematical analyses of the XPS spectra were carried out using the XPSpeak 4.1 computer software (RWM. Kwok, The Chinese University of Hong Kong).

2.3. Catalytic studies

The catalytic performances of the mixed metal oxides were evaluated in the selective oxidation of ammonia into nitrogen and water vapour (NH_3-SCO). The catalytic experiments were carried out under atmospheric pressure in a fixed-bed flow microreactor

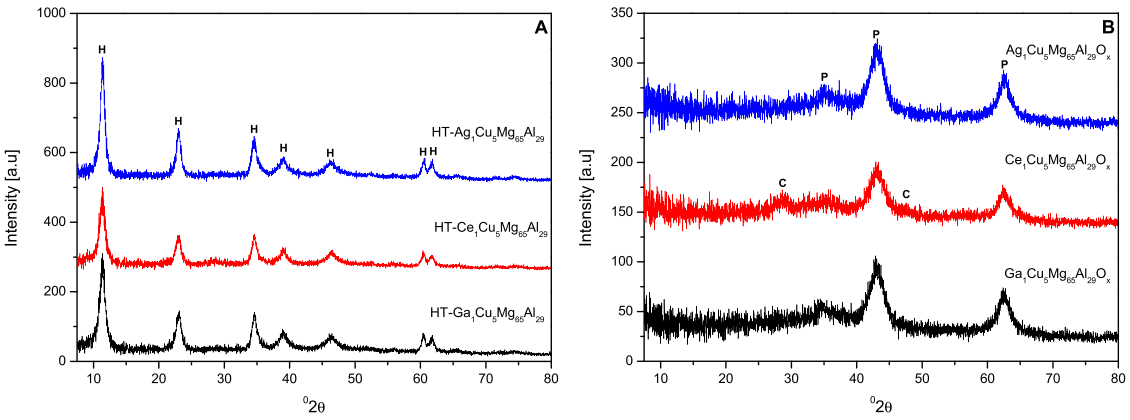

Fig. 1. Examples of X-ray diffraction patterns of the hydrotalcite-like compounds (A), and their calcined forms (B); H – hydrotalcite, P – periclase, MgO, C – fluorite, CeO_2.

(i.d., 6 mm; l., 320 mm). Prior to the reaction, the catalyst (100 mg) was outgassed at 500 °C for 1 h in a flow of pure argon (20 cm^3/min). The reactant concentrations at the reactor inlet: 0.5 vol.% NH_3, 2.5 vol.% O_2 and 97 vol.% Ar (40 cm^3/min; WHSV = 24,000 cm^3/h g), were continuously monitored using a QMS MKS, Cirrus 2 detector directly connected to the reactor outlet using a heated capillary. The measurements were performed in the temperature range of 100–500 °C with a linear heating rate of 5 K/min, and m/z values of 16 (NH_3), 28 (N_2), 30 (NO), 44 (N_2O), 46 (NO_2), 18 (H_2O). The signal of the argon line (m/z = 40) served as internal standard to compensate small fluctuations of the operating pressure. The sensitivity factors of the analysed lines were calibrated using commercial mixtures of gases.

The conversion of ammonia ($\alpha(NH_3)$) was determined using the following equation:

$$\alpha(NH_3) = \frac{C_0(NH_3) - C(NH_3)}{C_0(NH_3)} \times 100\%$$

where $C_0(NH_3)$ and $C(NH_3)$ – concentration of NH_3 in the inlet gas, and concentration of NH_3 in the outlet gas.

The desired reaction product is nitrogen, while undesired by-products are N_2O, NO, and NO_2.

The selectivity to N_2 ($S(N_2)$) was calculated taking into account all possible by-products based on the following equation:

$$S(N_2) = \frac{C(N_2)}{C(N_2) + C(N_2O) + \frac{1}{2}C(NO) + \frac{1}{2}C(NO_2)} \times 100\%$$

where $C(N_2)$, $C(N_2O)$, $C(NO)$, and $C(NO_2)$ – concentrations of N_2, N_2O, NO, and NO_2, respectively, in the outlet gases. The selectivity towards other possible by-products was obtained in an analogues way.

3. Results and discussion

The powder XRD diffraction patterns recorded for as-synthesized materials revealed pure crystalline hydrotalcite-like structures with rhombohedral $3R_1$ symmetry [34]. The thermal treatment of the hydrotalcite-like compounds led to complete destruction of the layered structure. After calcination at 600 °C, all materials possessed only reflections typical of poorly crystallized MgO-type oxides (reflections at about 36°, 43° and 63°) [11]. Exceptions were Ce-containing samples with $y \geq 0.75$, for which additional reflections appeared at about 29 and 48° corresponding to the fluorite CeO_2 phase [35]. Fig. 1 presents selected XRD patterns of the hydrotalcite-like compounds and their calcined forms, while Table 1 summarises the unit cell parameters of the hydrotalcite-like compounds. The lattice parameter a depends on the size of the cation in the brucite-like layers, while the parameter c refers to the interlayer thickness. The lattice parameter a increased with increasing Ag amount up to y = 0.25 and for Ce and Ga up to y = 0.75. The variance between a values in the series depends mainly on the ionic radii of the cations in octahedral coordination. Thus, among M^{3+} cations (0.102 nm Ce^{3+} versus 0.062 nm Ga^{3+} [36]), Ce-modified samples exhibited slightly higher a values

Table 1
Lattice parameters and mass losses of the TG–DTG for hydrotalcite-like precursors.

Sample codes	Cell parameter a [nm]	Crystallite size Da [nm]	Cell parameter c [nm]	Crystallite size Dc [nm]	Mass loss (step 1) [%]	Total mass loss [%]
HT-$Cu_5Mg_{66}Al_{29}$	0.3053	16	2.2944	20	16.02	42.22
HT-$Ag_{0.1}Cu_5Mg_{65.9}Al_{29}$	0.3058	10	2.3073	14	17.16	44.72
HT-$Ag_{0.25}Cu_5Mg_{65.75}Al_{29}$	0.3061	11	2.2770	15	15.17	42.94
HT-$Ag_{0.5}Cu_5Mg_{65.5}Al_{29}$	0.3060	15	2.3168	18	16.52	42.77
HT-$Ag_{0.75}Cu_5Mg_{65.25}Al_{29}$	0.3056	11	2.3038	18	15.53	42.81
HT-$Ag_1Cu_5Mg_{65}Al_{29}$	0.3056	11	2.3252	18	16.16	43.18
HT-$Ce_{0.1}Cu_5Mg_{65.9}Al_{29}$	0.3056	10	2.3250	14	16.44	44.79
HT-$Ce_{0.25}Cu_5Mg_{65.75}Al_{29}$	0.3061	10	2.3145	13	16.37	43.48
HT-$Ce_{0.5}Cu_5Mg_{65.5}Al_{29}$	0.3062	10	2.3132	15	15.45	42.94
HT-$Ce_{0.75}Cu_5Mg_{65.25}Al_{29}$	0.3064	10	2.3215	14	15.97	42.42
HT-$Ce_1Cu_5Mg_{65}Al_{29}$	0.3060	10	2.3276	13	16.46	43.12
HT-$Ga_{0.1}Cu_5Mg_{65.9}Al_{29}$	0.3061	12	2.3180	15	17.95	47.32
HT-$Ga_{0.25}Cu_5Mg_{65.75}Al_{29}$	0.3060	11	2.3217	14	17.34	45.05
HT-$Ga_{0.5}Cu_5Mg_{65.5}Al_{29}$	0.3060	10	2.3263	13	15.37	43.09
HT-$Ga_{0.75}Cu_5Mg_{65.25}Al_{29}$	0.3063	14	2.3217	14	17.15	43.91
HT-$Ga_1Cu_5Mg_{65}Al_{29}$	0.3058	7	2.3252	14	15.88	43.11

(with an exception of $Ce_{0.1}$–Cu–Mg–Al–O_x). Both lattice parameters *a* and *c* continued to change with $y \geq 0.25$ due to distortion induced by the further substitution of metals in the Cu–Mg–Al structure, and a possible partial segregation of metal species, which finally resulted in decreased crystallinity. A parameter *c* of about 2.3 nm stays characteristic for hydrotalcite-like materials containing carbonates located in the interlayer space [1]. The interlayer distances should increase upon decreasing electronegativity of the cations: Ga (1.82) > Cu (1.75) > Al (1.47) > Ag (1.42) > Mg (1.23) (according to Allred–Rochow scale) [37,38]. Cerium was not included in the scale, however, it stays between La (1.08) and Hf (1.23). Thus, upon increasing silver loading the parameter *c* should slightly increase compared to Cu–Mg–Al hydrotalcite-like compounds. The parameter *c* increased for $Ag_{0.25}$–Cu–Mg–Al–O_x. Additionally, we observed a significant variation in the parameter *c* among Ag-modified samples (significantly decreased and increased for $y = 0.25$ and 1, respectively). For Ce-based samples, the parameter *c* decreased up to $y = 0.5$, and for Ce-rich samples ($y \geq 0.75$) again increased. The Ga-containing samples showed an opposite trend. For these materials, the parameter *c* increased up to $y = 0.5$, then clearly decreased, and went up for Ga_1–Cu–Mg–Al–O_x. Velu et al. [39,40] reported a decrease of the parameter *c* with an incorporation of metals with higher oxidation state (M^{3+} and/or M^{4+}). Thus, it seems that besides electrostatic interactions – between the layer and the interlayer network after introduction of another cation into the Cu–Mg–Al structure – other factors regulate the parameter *c*. Since all as-synthesized materials contain CO_3^{2-} as interlayer anions, the interlayer water amount could influence *c* [38,41]. The studies showed a larger mass loss ($y \leq 0.75$) for Ga–Cu–Mg–Al hydrotalcite-like compounds. A possible explanation relates to the smaller ionic radius of Ga^{3+} probably leading to a higher amount of water molecules as well as anions located in the interlayer gallery.

Thermogravimetric analyses (TG–DTG) reflected the transformation of the hydrotalcite-like compounds into the corresponding mixed metal oxides. Jabłońska et al. [11,42] investigated the thermal decomposition of Cu–Mg–Al (5:66:29) that proceeded in two

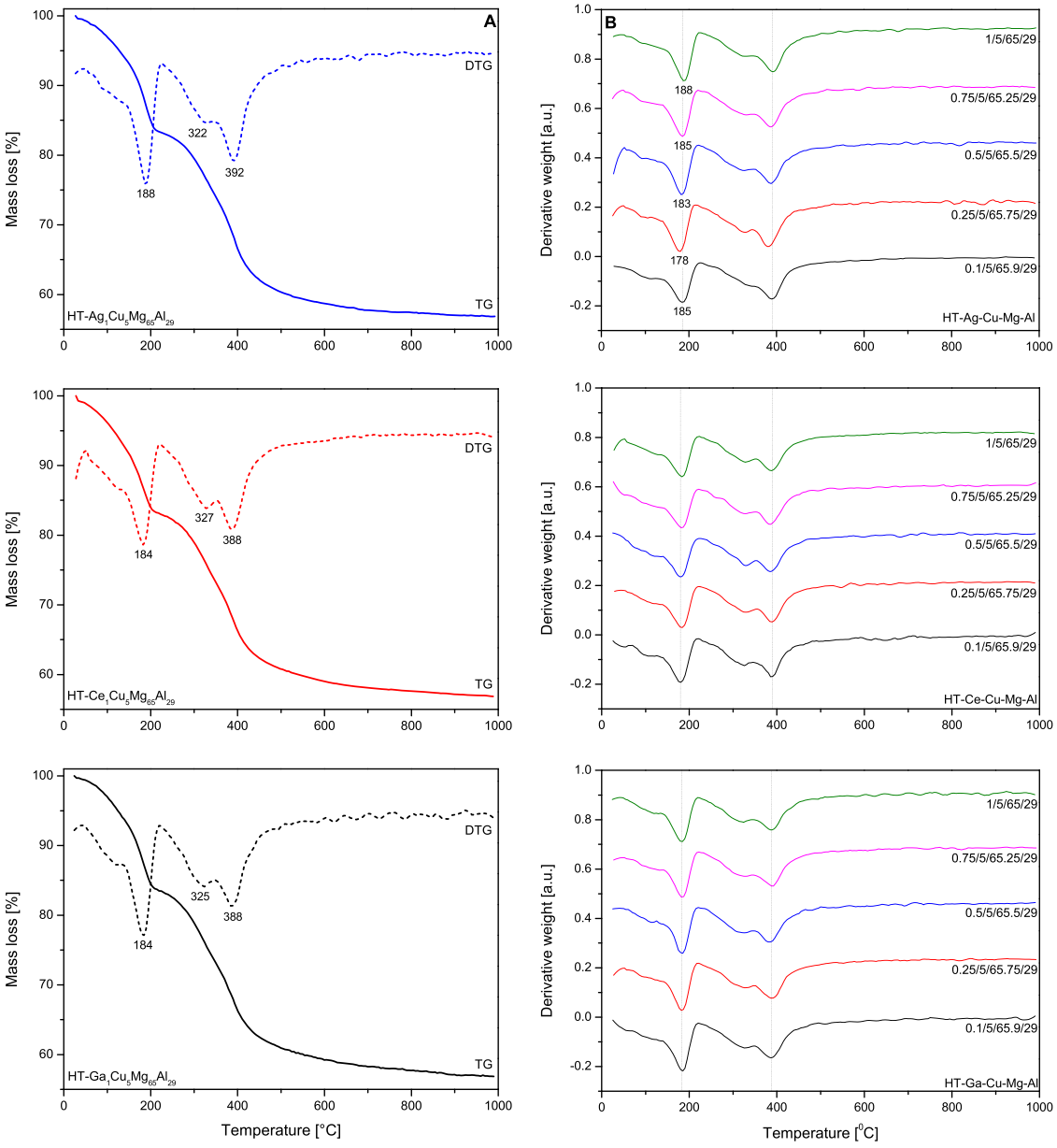

Fig. 2. Examples of TG–DTG of the hydrotalcite-like compounds (A), and comparison of DTG for the hydrotalcite-like compounds (B). Experimental conditions: mass of sample = 20 mg, flow of synthetic air = 10 cm^3/min, liner heating rate of 5 K/min.

Table 2
Specific surface area (S_{BET}), amount of chemisorbed ammonia (C_{NH_3}) and acid density (A_{NH_3}) of mixed metal oxides.

Sample codes	S_{BET} [m^2/g]/C_{NH_3} [mmol/g]/A_{NH_3} [mmol/m^2]					
y =	0	0.1	0.25	0.5	0.75	1.0
$Cu_5Mg_{66-y}Al_{29}O_x$	132/251/1.90					
$Ag_xCu_5Mg_{66-x}Al_{29}O_x$		151/262/1.74	154/271/1.76	155/274/1.77	158/282/1.78	161/288/1.79
$Ce_xCu_5Mg_{66-x}Al_{29}O_x$		234/699/2.99	238/649/2.73	240/406/1.69	243/370/1.52	247/359/1.45
$Ga_xCu_5Mg_{66-x}Al_{29}O_x$		216/388/1.80	222/400/1.80	232/421/1.81	244/438/1.80	248/406/1.64

main stages with a total mass loss of about 43 wt.%. The DTG peak centred at 184 °C corresponded to the removal of interlayer and weakly adsorbed water without collapse of the hydrotalcite-like structure. The second region manifested by two unresolved DTG minima at 320 and 374 °C were related to the weight loss due to the dehydroxylation of the brucite-like layers and thermal decomposition of interlayer anions (carbonates and trace nitrates). Moreover, copper introduced into the hydrotalcite-like structure stabilized CO_3^{2-} anions that decomposed above 600 °C. As depicted on Fig. 2, the thermal decomposition of the modified hydrotalcite-like compounds proceeded in an analogous way to the reference Cu–Mg–Al–O_x. All materials exhibited a weight loss in the range of 42–48% of the initial weight up to 1000 °C. The introduction of Ag, Ce or Ga within the hydrotalcite-like structure facilitated the decomposition processes of the hydrotalcite-like structure. The first DTG minimum stage (the removal of interlayer and weakly absorbed water) shifted to lower temperatures for all materials compared to dehydroxylation and decomposition of interlayer anions. However, the temperatures of decomposition varied depending on the metal introduced into the brucite-like layers and its loading. For Ag–Cu–Mg–Al materials the temperature of both minima decreased up to $y = 0.25$, and subsequently increased. Thus, a higher Ag loading ($y \geq 25$) retarded the transformation of hydrotalcite-like compounds into mixed metal oxides. Such a tendency did not appear for Ce(Ga)–Cu–Mg–Al hydrotalcite-like compounds, possibly due to the smaller ionic radii of these M^{3+} cations (Ce^{3+} or Ga^{3+}) in octahedral coordination compared to Ag^+ (0.115 nm [36]). Both Ce- and Ga-containing samples ($y = 0.1–1$) showed similar temperatures for water removal, the loss of hydroxyl groups from the brucite-like layers and decomposition of anions. Das et al. [43] found that an increasing Ce content in Mg-Al hydrotalcite-like compounds (Ce:Mg:Al = 1.5:73:25.5, 3.5:74:22.5, 5.5:76:18.5, 10:73:17) facilitated the removal of water, while the second process shifted to higher temperatures. On the other side, Sun et al. [44] reported that increasing M^{3+} (Ga^{3+}) in the Mg–Al matrix (Ga:Mg:Al = 2:100:8, 33:100:0) led to a shift of the first minimum to higher temperature due to tightly bound water. Opposite, an increased Ga-loading favoured the decomposition of hydrotalcite-like compounds into mixed metal oxides, thus the second minimum shifted to lower temperatures. We did not observe similar changes for our Ga–Cu–Mg–Al nor Ce–Cu–Mg–Al materials possibly due to a lower amount of the incorporated M^{3+}.

Table S1 (Supplementary Information) gathers results of the chemical analysis of selected mixed metal oxides. The determined molar ratios were very similar to the intended ratios, however with small deficiency of magnesium and excess of aluminium. The specific surface areas (S_{BET}), the amount of chemisorbed NH_3(C_{NH_3}) and acid density (A_{NH_3}) varied depending on the composition of hydrotalcite derivatives. Table 2 summarises the values of S_{BET}, C_{NH_3} and A_{NH_3} of the mixed metal oxides, while Fig. 3 presents examples of ammonia desorption curves. Cu–Mg–Al–O_x exhibited 132 m^2/g and adsorbs 251 μmol/g ammonia, yielding an acid density of 1.90 μmol/m^2. The specific surface area and amount of chemisorbed ammonia increased for Ag-, Ce-, or Ga-modified mixed metal oxides with increasing metal content. Compared to Cu–Mg–Al–O_x, the improved properties were more distinct for Ga- or Ce-containing materials (234–247 or 216–248 m^2/g) than for Ag-modified samples (151–161 m^2/g). Obviously, introducing other metals within the coprecipitation step facilitated the formation of materials with improved textural properties. Also, Pérez et al. [45] reported an increase of S_{BET} for Cu–Co–Mg–Al–O_x (209 m^2/g) compared to Cu–Mg–Al–O_x (155 m^2/g) or Co–Mg–Al–O_x (172 m^2/g). Furthermore, Wang et al. [20] provided similar conclusions related to Ce–Cu–Mg–Al–O_x (50 m^2/g) compared to Cu–Mg–Al–O_x (44 m^2/g). The isotherms of the obtained mixed metal oxides exhibited the characteristic type IV shape (not shown), which together with the pore size distribution results, suggested that the samples were mesoporous materials (60–62 Å).

All obtained Ag-, Ce-, or Ga-containing mixed metal oxides exhibited similar NH_3-TPD profiles. The NH_3 desorption patterns were spread between 70 and 350 °C with a maximum at 150–160 °C. With an increasing amount of Ag, Ce or Ga the amount of chemisorbed ammonia of Cu–Mg–Al–O_x increased. According to Vulic et al. [46], the desorption temperatures enable conclusions regarding the strength of Lewis acid sites of hydrotalcite derived mixed metal oxides. Thus, all mixed metal oxides evaluated in our studies revealed sites of similar strength; however, the strength of acid sites slightly increased from Ag- and Ce-based materials up to Ga-based samples. Ga–Cu–Mg–Al–O_x ($y \geq 0.5$) showed a significantly higher acidity than analogous Ag-, or Ce-doped mixed metal oxides. However, the amount of chemisorbed ammonia together with acid density decreased for Ga_1–Cu–Mg–Al–O_x. Similarly, as the loading of ceria increased the amount of chemisorbed ammonia decreased due to phases segregation (bulk CuO_x and/or CeO_2) of Ce–Cu–Mg–Al–O_x at $y > 0.25$. In line, the acid density gradually decreased for those materials. As revealed by XRD analysis, CeO_2 finally segregated for Ce-rich samples ($y \geq 0.75$).

Table 3
Maximum temperatures of the reduction peak (T_{red}) and amounts of H_2 theoretical and consumed during TPR measurements (H_2 uptake) of mixed metal oxides.

Sample codes	T_{red} [°C]/H_2 uptake [mmol/g][a]/Theoretical H_2 uptake [mmol/g][b]					
y =	0	0.1	0.25	0.5	0.75	1.0
$Cu_5Mg_{66-y}Al_{29}O_x$	340/0.81/1.10					
$Ag_xCu_5Mg_{66-x}Al_{29}O_x$		333/1.20/1.12	330/1.37/1.15	320/1.11/1.20	311/1.14/1.25	315/1.14/1.30
$Ce_xCu_5Mg_{66-x}Al_{29}O_x$		315/1.24/1.12	319/1.21/1.15	320/1.21/1.20	270;313/1.41/1.24	270;311/1.26/1.29
$Ga_xCu_5Mg_{66-x}Al_{29}O_x$		310/1.43/1.12	317/1.33/1.15	312/1.34/1.21	313/1.33/1.26	323/1.29/1.31

[a] Calculated by equation: $Y = 9E{-}09X + 2E{-}07$, $R^2 = 0.9996$, and X, Y referred to the area of each reduction peak and the H_2 consumption, respectively.
[b] Calculated amount of H_2 to be consumed for the complete reduction of Cu^{2+}, Ag^+, Ce^{3+}, Ga^{3+} to their metallic forms.

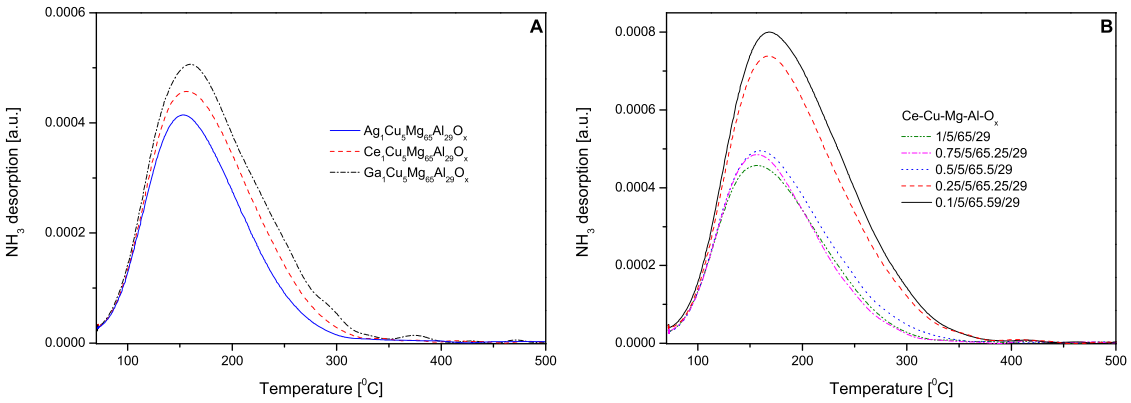

Fig. 3. Examples of NH_3-TPD profiles of mixed metal oxides (A), and series of Ce–Cu–Mg–Al–O_x (B). Experimental conditions: mass of sample = 100 mg, sorption: [NH_3] = 1.0 vol.%, [Ar] = 99.0 vol.%; desorption: [Ar] = 100.0 vol.%; total flow rate = 20 cm^3/min, linear heating of 5 K/min.

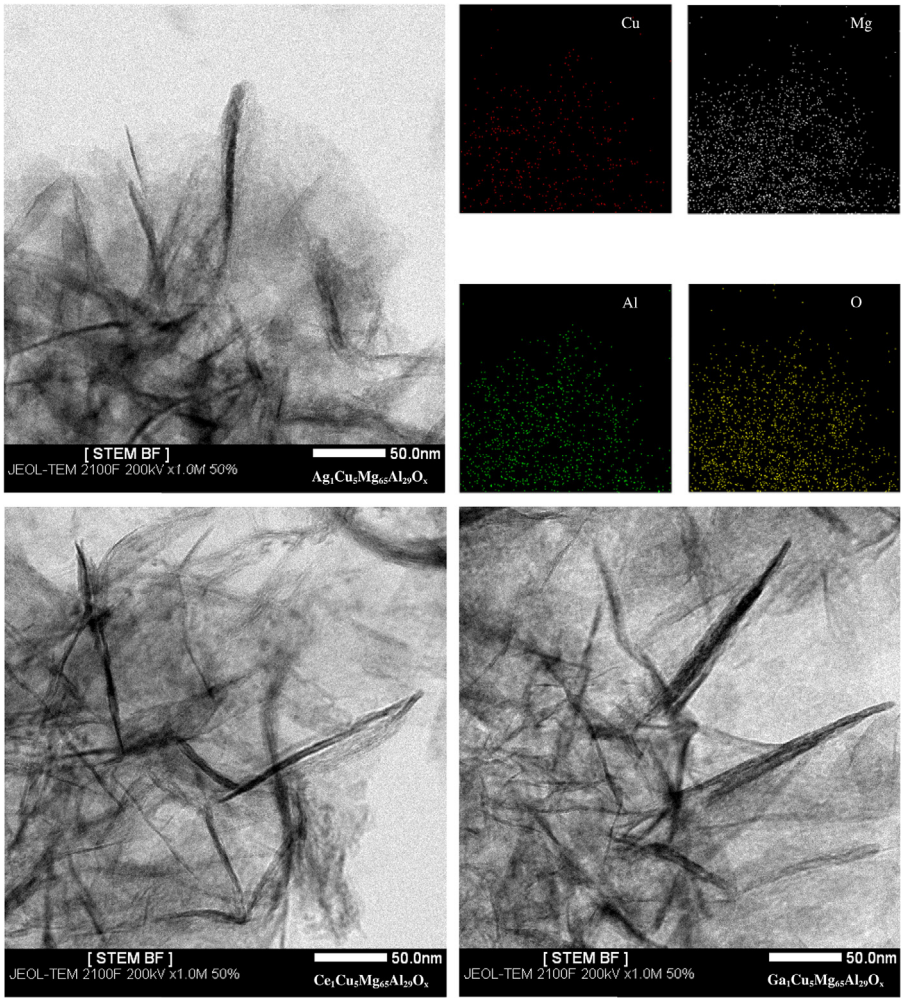

Fig. 4. Examples of STEM images of mixed metal oxides and EDX analysis for Ag_1–Cu–Mg–Al–O_x.

The transmission electron microscopy analyses evidenced the morphology of the obtained mixed metal oxides. The hydrotalcite-like compounds have a lamellar structure [47,48]. Fig. 4 shows TEM micrographs of selected mixed metal oxides. A lamellar morphology of hydrotalcite-like compounds preserved after calcination at 600 °C and whisker-like particles were detected in all analysed mixed metal oxides. EDX measurements confirmed the uniform distribution of the components of the mixed metal oxides.

The nature and amount of introduced metals also influenced the redox properties of the mixed metal oxides. Fig. 5 presents H_2-TPR profiles obtained for all studied mixed metal oxides, while Table 3 lists the maximum temperatures of the reduction peaks (T_{red}), and the theoretical and indeed consumed amounts of hydrogen during the measurements (H_2 uptake). A quantitative analysis on H_2 consumption was carried out by integrating the H_2-TPR curves. The profile obtained for Cu–Mg–Al–O_x consisted of a sharp peak at about 340 °C, attributed to the reduction of CuO

to metallic copper ($Cu^{2+} \rightarrow Cu^0$), together with a broad maximum around 600 °C ascribed to the hydrogenation of residual carbonates ($M\text{-}CO_3 + 4H_2 \rightarrow M\text{-}O + CH_4 + 2H_2O$) [11,42]. The reduction temperature of Cu–Mg–Al–O_x decreased for Ag-, Ce-, or Ga-modified mixed metal oxides; however, the temperature shift depended on the metal loading. For all mixed metal oxides an intensive reduction peak appeared in the H_2-TPR profiles at about 301–333 °C due to the reduction of CuO_x to Cu^0. The incorporation of an increasing amount of Ag led to a shift of the peak maximum to about 20 K lower temperatures (from 333 °C for $Ag_{0.1}$–Cu–Mg–Al–O_x to 315 °C for Ag_1–Cu–Mg–Al–O_x), as well as changes of the character of the profile (from sharp to broadened for $y = 1$). Thus, the reducibility increased for Ag-containing samples up to $y = 0.25$, and then subsequently decreased (H_2 uptake of 1.11 mmol/g for $y = 0.5$). $Ag_{0.75}$–Cu–Mg–Al–O_x revealed the lowest reduction temperature for Ag-modified samples, indicating the appearance of surface copper oxide species [49]. An increase in Ag loading favoured the formation of bulk CuO_x [7,13], indicating a diminished dispersion of copper oxides species (bulk profile shape). The results suggested that the introduction of a proper amount of Ag (up to $y = 0.25$) facilitated a high dispersion of copper oxides species.

The reduction temperature in Ce–Cu–Mg–Al mixed metal oxides increased from 315 °C for $y = 0.1$ to 319–320 °C for $y = 0.25$–0.5. The shift of the H_2-TPR profile to higher temperatures corresponds to a decreasing reducibility of CuO_x. However, for samples with $y \geq 0.75$, the H_2-TPR profiles revealed a split into bimodal peaks. The main reduction peak appeared at 313 and 311 °C for $y = 0.75$ and $y = 1$, respectively. A small shoulder arose at 270 °C. Thus, a higher Ce content favoured the reduction of CuO_x accompanied by a higher H_2 consumption (1.26–1.41 mmol/g). According to XRD analysis, CeO_2 segregated for Ce-rich samples ($y \geq 0.75$), which possibly caused the difference in CuO_x reducibility. The broad shoulder arose possibly due to the reduction of finely dispersed copper oxides species strongly interacting with cerium cations (Ce^{4+}), whereas the main peak reflected the reduction of bulk copper oxide species [24]. Thus, a certain amount of Ce (up to $y = 0.25$) incorporated into Cu–Mg–Al–O_x enhanced the dispersion of CuO_x. Such findings remained valid also in case of Ga-modified materials. Ga–Cu–Mg–Al–O_x presented a similar trend with a sharp H_2-TPR profile up to $y = 0.25$. Subsequently, the H_2-TPR profile became closer to the shape corresponding to bulk species reduction for Ga-rich samples ($y \geq 0.5$). The increasing Ga-loading showed a retarding impact on the reduction of CuO_x; however, this trend was interrupted for $Ga_{0.25}$–Cu–Mg–Al–O_x. The reduction temperature of CuO_x increased from 310 °C with increasing gallium loading up to 317 °C for $y = 0.25$. Afterwards, the reduction temperature decreased for $Ga_{0.5}$–Cu–Mg–Al–O_x possibly due to formation of surface CuO_x species with higher reducibility [49]. For Ga-rich samples ($y \geq 0.75$), the reduction temperature increased up to 323 °C due to formation of bulk CuO_x [7,13]. Overall, the content of Ag, Ce or Ga equal to 0.25 resulted in the formation of monodisperse, easily reducible CuO_x.

The nature of the metal (Ag, Ce, Ga, Cu) species on the surface was verified using X-ray photoelectron spectroscopy for selected mixed metal oxides. Fig. 6 shows Cu 2p and O 1s XPS spectra of the mixed metal oxides, and Table 4 summarises positions of binding energies, full-width at half-maximum (FWHM), peak areas and molar ratios. Ag, Ce and Ga were not detected due to their low concentrations in the mixed metals oxides. Cu–Mg–Al–O_x exhibited a profile consisting of the main peak at about 933 eV without satellite peaks, which are characteristic for Cu^{2+} species [50]. The presence of Cu^+ and/or Cu^0 species on the surface of Cu–Mg–Al–O_x was related to the reduction of Cu^{2+} under vacuum. The low copper concentration on the surface of this sample (peak area of 3198.1, Cu/(Al + Mg) molar ratio of 0.61) indicated that most

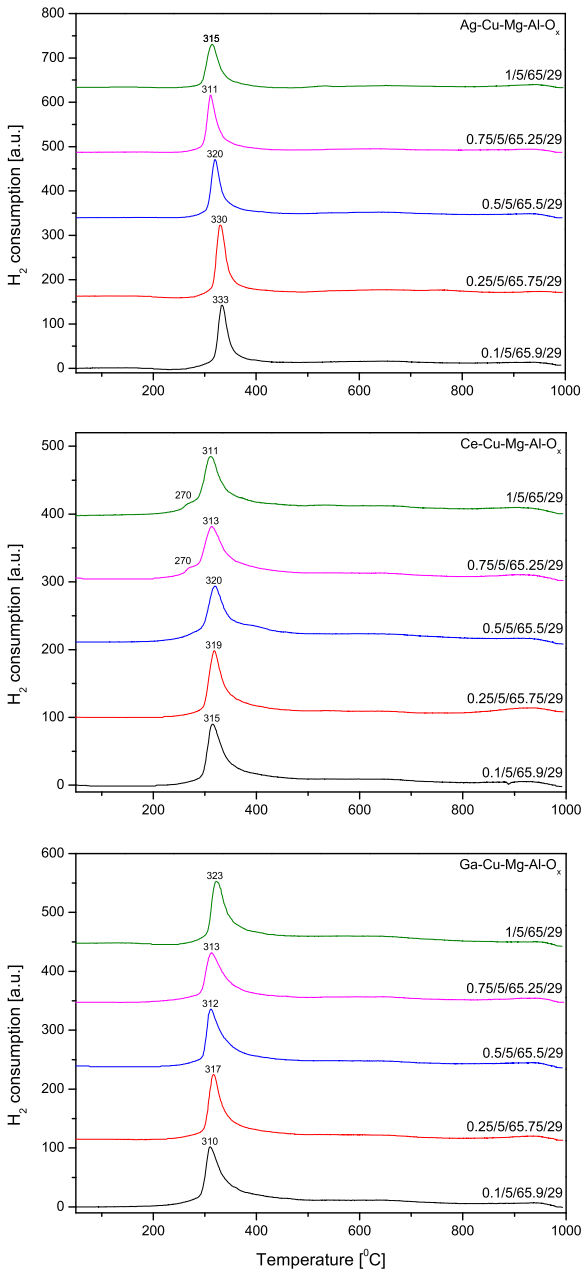

Fig. 5. Results of H_2-TPR studies for the mixed metal oxides. Experimental conditions: mass of catalysts = 30 mg, [H_2] = 5.0 vol.%, [Ar] = 95.0 vol.%, flow rate = 25 cm^3/min, linear heating of 5 K/min.

Cu^{2+} species were in the mixed oxide matrix. The strong shake-up satellite peaks at about 961 and 942 eV appeared for all Ag(Ce, Ga)-Cu systems, thus Cu^{2+} species appeared on the surface of these bimetallic catalysts. The position of Cu 2p binding energies for the Ag, Ce- or Ga-modified Cu–Mg–Al–O_x shifted to higher values for metal-rich samples ($y = 1$). The effect was more evident for Ce- and Ga-modified samples (933.4 and 933.0 eV, respectively). Consequently, Cu^{2+} species observed in these materials existed mainly in the form of bulk CuO_x [51]. In a similar manner, the Cu/(Al + Mg) molar ratio decreased for Ce- and Ga-rich samples ($y = 1$). On the other hand, the Cu/(Al + Mg) molar ratio increased from 0.87 to 1.00 for Ag–Cu–Mg–O_x with $y = 0.25$ and 1, respectively. These results appeared possibly due to higher ionic radii of Ag^+ than Ce^{3+} or Ga^{3+} in octahedral coordination pushing copper oxide species outside the mixed oxide matrix in Ag_1–Cu–Mg–Al–O_x.

Table 4
Positions of binding energies, full width at half-maximum (FWHM), peak areas and molar ratios for selected mixed metal oxides.

Sample codes	Peak Position/FWHM [eV]		Peak area [a.u.]		Molar ratio[a]	
	Cu 2p	O 1s	Cu 2p	O 1s	$O_\alpha/(O_\beta+O_\gamma)$	Cu/(Al+Mg)
$Cu_5Mg_{66}Al_{29}O_x$	933.2/4.5	532.6/2.2	3198.1	5521.8	0.31	0.61
		530.9/2.4		13922.5		
		529.0/2.3		6062.4		
$Ag_{0.25}Cu_5Mg_{65.75}Al_{29}O_x$	961.0/3.0	532.1/2.3		12988.7	0.11	0.87
	942.6/3.0	530.3/2.8		41135.6		
	932.7/3.7	528.4/1.9	7917.6	6041.8		
$Ag_1Cu_5Mg_{65}Al_{29}O_x$	961.0/3.0	532.1/2.3		10918.9	0.14	1.00
	942.6/3.0	530.3/2.7		3430.4		
	932.8/3.9	528.4/2.1	8060.1	6296.4		
$Ce_{0.25}Cu_5Mg_{65.75}Al_{29}O_x$	961.0/6.0	532.1/2.4		13370.9	0.16	1.14
	942.6/4.7	530.2/2.8		40493.8		
	932.9/4.1	528.4/2.2	10921.6	8674.9		
$Ce_1Cu_5Mg_{65.75}Al_{29}O_x$	961.0/4.0	532.4/2.6		16129.9	0.18	0.87
	942.6/4.0	530.6/2.5		31416.9		
	933.4/4.0	528.9/2.1	8321.6	8357.9		
$Ga_{0.25}Cu_5Mg_{65.75}Al_{29}O_x$	961.0/3.0	532.5/2.3		7408.8	0.23	0.91
	942.6/3.0	530.5/2.9		41943.9		
	932.7/3.9	528.6/2.3	10123.2	11084.8		
$Ga_1Cu_5Mg_{65}Al_{29}O_x$	961.0/4.0	532.3/2.5		12089.8	0.09	0.88
	942.6/4.0	530.3/2.8		39097.1		
	933.0/3.7	528.5/1.9	8823.6	4454.3		

[a] Estimated from the integrated areas of the respective XPS peaks.

Table 5
Comparison of the results of catalytic tests (T_{100} temperature needed for 100% of NH_3 conversion).

Sample codes	T_{100} [°C]	N_2 selectivity	NO selectivity	N_2O selectivity
		at T_{100} [%]		
$Cu_5Mg_{66}Al_{29}O_x$	500	86	11	3
$Ag_{0.1}Cu_5Mg_{65.9}Al_{29}O_x$	425	89	5	6
$Ag_{0.25}Cu_5Mg_{65.75}Al_{29}O_x$	425	90	4	6
$Ag_{0.5}Cu_5Mg_{65.5}Al_{29}O_x$	425	90	4	6
$Ag_{0.75}Cu_5Mg_{65.25}Al_{29}O_x$	425	92	3	5
$Ag_1Cu_5Mg_{65}Al_{29}O_x$	400	91	2	7
$Ce_{0.1}Cu_5Mg_{65.9}Al_{29}O_x$	400	91	2	7
$Ce_{0.25}Cu_5Mg_{65.75}Al_{29}O_x$	400	91	2	7
$Ce_{0.5}Cu_5Mg_{65.5}Al_{29}O_x$	400	88	5	7
$Ce_{0.75}Cu_5Mg_{65.25}Al_{29}O_x$	400	91	4	5
$Ce_1Cu_5Mg_{65}Al_{29}O_x$	400	91	5	4
$Ga_{0.1}Cu_5Mg_{65.9}Al_{29}O_x$	375	90	3	7
$Ga_{0.25}Cu_5Mg_{65.75}Al_{29}O_x$	375	91	3	6
$Ga_{0.5}Cu_5Mg_{65.5}Al_{29}O_x$	375	90	4	6
$Ga_{0.75}Cu_5Mg_{65.25}Al_{29}O_x$	400	90	3	7
$Ga_1Cu_5Mg_{65}Al_{29}O_x$	450	93	2	5

The O 1s spectra of the mixed metal oxides were deconvoluted to lattice oxygen O_α (528–529 eV), chemisorbed oxygen O_β (530–531 eV), and adsorbed OH groups O_γ (532–533 eV) [52]. The lattice oxygen O^{2-} interacts with copper with formation of Cu–O bonds. As evidenced from H_2-TPR analysis, the strength of these bonds varied within mixed meal oxides. Accordingly, $Ga_{0.25}$–Cu–Mg–Al–O_x revealed the highest area and $O_\alpha/(O_\beta+O_\gamma)$ molar ratio of the lattice oxygen (peak area of 11,084.8, molar ratio of 0.23), and the lowest temperature of the H_2-TPR peak. The comparison between Ce-containing catalysts revealed a higher amount of lattice oxygen for the sample with $y = 0.25$ than 1 (peak area of 8674.9 versus 8357.9, respectively). Shan et al. [53] or Talukdar et al. [54] claimed that the redox cycle – involving the synergistic interactions between Ce^{3+} and Cu^{2+} ($Ce^{3+} + Cu^{2+} \rightarrow Ce^{4+} + Cu^{+}$) – released the lattice oxygen. As confirmed by XRD and H_2-TPR analysis for samples with higher cerium content ($y \geq 0.75$), bulk CeO_2 and CuO appeared, thus the interaction occurred only on the interface of these phases.

The obtained Ag(Ce, Ga)–Cu–Mg–Al hydrotalcite derived mixed metal oxides were tested as catalysts for selective oxidation of ammonia into nitrogen and water vapour (NH_3-SCO). N_2O, NO and NO_2 appeared as by-products. Figs. 7 and 8 present the results for the experiments performed over selected Ag(Ce, Ga)–Cu–Mg–Al–O_x, whereas Table 5 gathers the results of catalytic tests at temperature T_{100}, (temperature at which 100% ammonia conversion was reached). For Cu–Mg–Al–O_x the oxidation of ammonia from the reaction mixture started at about 150 °C, and reached full conversion at 500 °C with high N_2 selectivity (>85%) (Fig. S1, Supplementary Information). For Ag-containing catalysts the ammonia oxidation started at about 150 °C, and about 400–425 °C were sufficient to obtain full NH_3 conversion. N_2 remained the main reaction product in the whole temperature range of 100–500 °C; however, other by-products (NO and N_2O) appeared above 300 °C. The selectivity to N_2 decreased mainly due to the formation of NO, especially for Ag-rich samples ($y \geq 0.5$) (Fig. S2). The selectivity to NO reached up to 21% above 425 °C for Ag_1–Cu–Mg–Al–O_x. Chmielarz et al. [11] showed a similar behaviour over Cu–Mg–Al–O_x modified with other noble metals (Pt, Pd, Rh), that correlate to the *Internal Selective Catalytic Reduction* (*i-SCR*) mechanism of NH_3-SCO. Briefly, a part of ammonia is oxidized to NO, however, an excess of ammonia exists at low temperatures (<375 °C) due to the low rate of the ammonia oxidation. The gen-

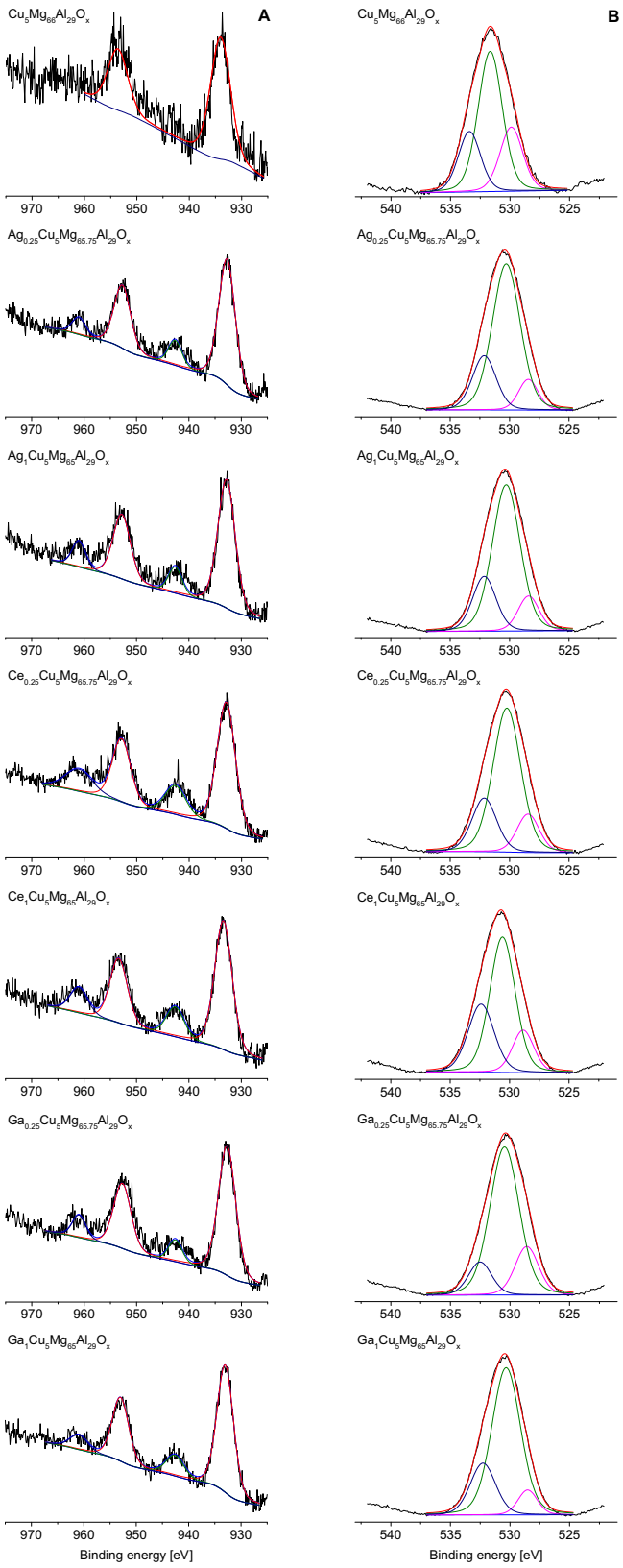

Fig. 6. Examples of XPS spectra of mixed metal oxides: Cu 2p XPS spectra (A), and O 1s XPS spectra (B).

erated NO reacts with residual NH_3 with formation of N_2 and/or N_2O. At higher temperatures (>375 °C), the ammonia conversion increased resulting in limited residual ammonia able to completely reduce generated NO. Therefore, the selectivity to N_2 and/or N_2O decreased, with subsequent formation of NO. Noble metals serve as active catalysts in ammonia oxidation into NO; thus, the selectivity to NO increases with increasing Ag loading.

For Ce-based catalysts, the ammonia oxidation started at around 150 °C, while full ammonia conversion occurred at 400 °C. Besides N_2, N_2O, and NO, NO_2 appeared as minor by-product for samples with Ce loading up to $y = 0.5$. N_2 remained the major product below 400 °C, while at higher temperatures NO dominated, especially for $y = 0.1$–0.5. Interestingly, $Ce_{0.25}$–Cu–Mg–Al–O_x showed a lower tendency for NO formation than $Ce_{0.5}$–Cu–Mg–Al–O_x in the range of 400–500 °C. For Ce-rich catalysts ($y \geq 0.75$), the N_2 selectivity increased to above 70% over Ce_1–Cu–Mg–Al–O_x (Fig. S2). Wang et al. [24] studied CuO–CeO_2 prepared by a surfactant-templated method, and found N_2 as the dominant product, while N_2O and NO were the only detected by-products of NH_3-SCO in the range of 180–300 °C; thus, lower temperatures than in our studies. Also, other researchers did not detect NO_2 over CuO–CeO_2 catalysts with bulk phases of copper and cerium oxides [e.g. [55,56]]. We detected a minor amount of NO_2 for materials with $y \leq 0.5$) above 400 °C. As depicted in NH_3-TPD and XPS results, a strong interaction between copper and cerium (Cu^{2+}/Cu^{+} and Ce^{4+}/Ce^{3+}) in Ce–Cu–Mg–Al–O_x ($y \leq 0.5$) led to enhanced adsorption of NH_3 molecules. Subsequently, the lattice oxygen at the surface of the catalysts oxidized the chemisorbed ammonia into NO, which partially transformed to NO_2. However, for bulk CuO_x (as evidenced by H_2-TPR and XPS studies), the selectivity to all by-products decreased (no NO_2 was detected during the catalytic tests), while N_2 started to be the main product between 100 and 500 °C. Consequently, the activity decreased for Ce-rich materials. The *i-SCR* mechanism was proposed over CuO–CeO_2 catalysts, where ceria led to the formation of NO_x [24]. This is consistent with our results as we observed the production of NO and NO_2 above 400 °C. Thus, the oxidation of ammonia into NO_x is rate-limiting in the low temperature range.

Full ammonia oxidation over Ga-containing catalysts appeared at significantly lower temperatures (375 °C, $y \leq 0.5$) than for analogues Ag- or Ce-based catalysts. The selectivity to N_2 increased with increasing gallium content and reached above 80% between 100 and 500 °C over $Ga_{0.25}$–Cu–Mg–Al–O_x. For Ga-rich materials ($y \geq 0.5$), the product distribution changed, however N_2 remained the main product (Fig. S2). For Ga_1–Cu–Mg–Al–O_x, the activity dropped significantly (full conversion at 450 °C) along with a simultaneous increase in N_2 selectivity (above 90% up to 500 °C). The increase in N_2 selectivity appears to be related to lower reducibility of CuO_x (based on H_2-TPR and XPS analyses).

To the best of our knowledge, until now no reports refer to Ga–Cu systems dedicated to NH_3-SCO. Thus, the role of gallium on the catalytic performance in ammonia oxidation could not be clarified yet. However, we observed a similar trend of catalytic performance as for related Ce-obtaining samples. Thus, the role of gallium in Ga–Cu bimetallic oxide system could be alike. The *i-SCR* mechanism was proposed for Ag–Cu and Ce–Cu hydrotalcite derived mixed metal oxides, however, it seems to be valid for other combinations of metals with CuO_x as well.

Overall, Ag-, Ce-, or Ga-promoted catalysts reached enhanced catalytic performance compared to the reference Cu–Mg–Al–O_x (full conversion at 500 °C with 86% N_2 selectivity). In detail, Ga-promoted catalysts reached higher catalytic performance than catalysts modified with Ag and Ce up to $y \leq 0.5$. The optimum activity was reached over $Ga_{0.25}$–Cu–Mg–Al–O_x with full conversion at 375 °C and 91% N_2 selectivity at this temperature. The analogues $Ag_{0.25}$–Cu–Mg–Al–O_x and $Ce_{0.25}$–Cu–Mg–Al–O_x reached complete NH_3 conversion at higher temperatures of about 50 and 25 K,

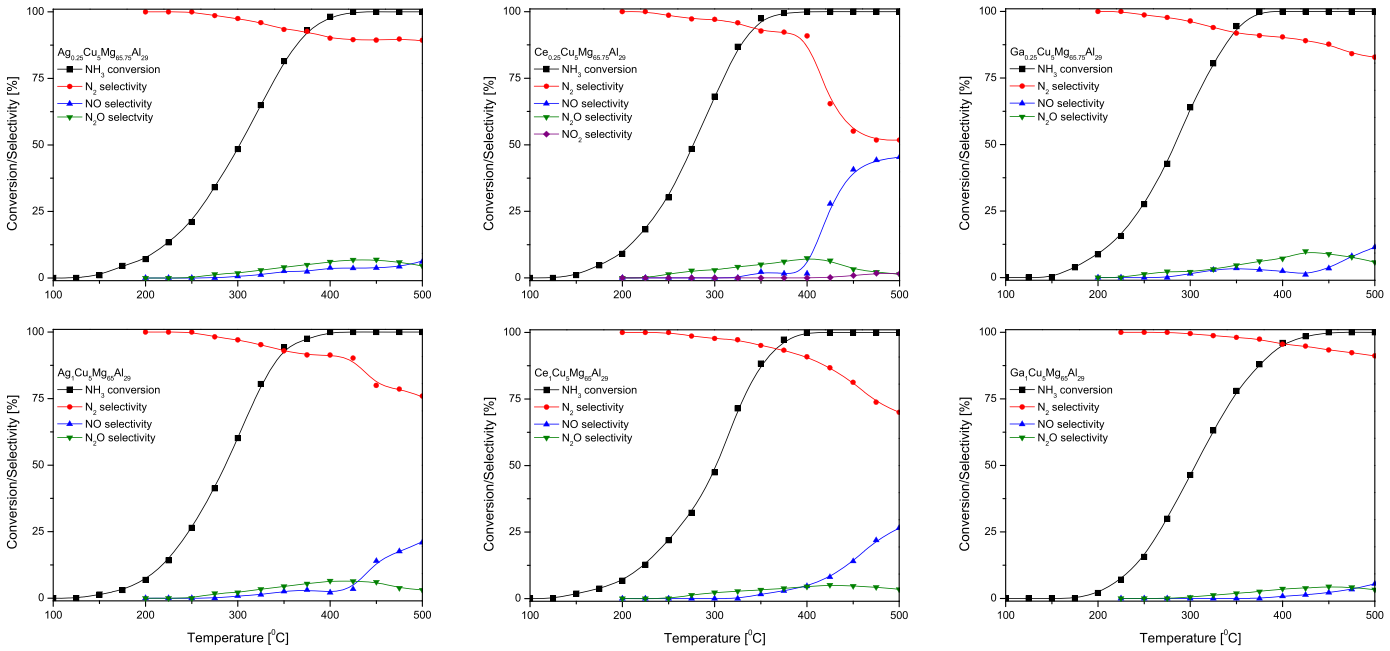

Fig. 7. Results of catalytic tests for NH_3-SCO performed over mixed metal oxides. Experimental conditions: mass of catalysts = 100 mg, [NH_3] = 0.5%, [O_2] = 2.5%, [Ar] = 97%, total flow rate = 40 cm^3/min, WHSV = 24,000 cm^3/h g, linear heating of 5 K/min.

respectively, with similar N_2 selectivity. Taking into account catalysts with $y = 1$, the conversion of Ga-modified sample decreased significantly, while N_2 remained the main reaction product in the whole temperature range (full conversion at 450 °C with 93% N_2 selectivity). Ag- and Ce-containing catalysts showed similar profiles, with slightly higher selectivity to N_2 above 400 °C over Ag_1–Cu–Mg–Al–O_x.

The surface acidity did not significantly influence the catalytic performance of the hydrotalcite derived mixed metal oxides. Jabłońska et al. [10] investigated Cu–Mg–Al–O_x with varying Mg:Al molar ratios and found that catalysts with higher Al-content in the samples revealed a slight increase in the N_2 selectivity at higher temperatures (above 450 °C). Higher acidity of the catalysts had also no distinct influence on activity. In addition, for the studied Ga–Cu–Mg–Al–O_x, the catalytic performance did not correlate with the increasing amount of chemisorbed ammonia or acid density. Other researchers working on NH_3-SCO reported redox-performance correlations [24,57,58]. Wang et al. [24] found a correlation between the uniformly dispersed CuO_x species and catalytic activity over CuO–CeO_2. A higher ratio of finely dispersed copper oxides species guaranteed enhanced catalyst activity. Curtin and Lenihan [58] reported a linear correlation between the catalysts activity and the H_2-TPR reduction temperature for copper-exchanged zeolites. The most active catalysts exhibited the lowest reduction temperature. This remains in line with studies of Jabłońska et al. [11,57] over noble metal (Pt, Pt, Rh) modified copper-based catalysts, including Cu–Mg–Al hydrotalcite derived mixed metal oxides. Therein, for lower reduction temperature activity increased, while N_2 selectivity decreased, especially in the higher temperature range (above 375 °C).

Introducing Ag, Ce or Ga within the Cu–Mg–Al–O_x structure significantly modified its redox properties in accordance with the used amount of metal. Ag-based samples showed a decreasing reduction temperature for CuO_x species with increasing Ag content up to 0.75. Catalysts with $y = 0.1$ and 0.25 were reduced at similar temperatures, while a slightly higher N_2 selectivity (between 400 and 500 °C) was reached over $Ag_{0.25}$–Cu–Mg–Al–O_x with easily reducible CuO_x (a sharp H_2-TPR profile). The activity increased as the maximum reduction temperature decreased ($y \leq 0.75$). An exception stayed Ag_1–Cu–Mg–Al–O_x that reached a reduction temperature slightly higher than for $y = 0.75$. The H_2-TPR profile of Ag_1–Cu–Mg–Al–O_x revealed a rather bulk character of CuO_x, indicating possible phase segregation – including Ag_2O – that caused higher catalytic activity and the observed drop in N_2 selectivity. Also Yang et al. [59] confirmed a higher activity and lower N_2 selectivity of Ag-based catalysts (with crystallized Ag_2O) than Ag–Cu bimetallic systems. For Ce-modified catalysts the reduction temperature increased up to $y = 0.5$ (from 315 to 320 °C), however, the activity remained nearly constant. $Ce_{0.25}$–Cu–Mg–Al–O_x revealed a higher amount of easily reducible CuO_x (a sharp H_2-TPR profile) than $Ce_{0.5}$–Cu–Mg–Al–O_x (slightly bulk profile), thus, also slightly higher selectivity to N_2. Afterwards, the reduction temperature decreased due to phases segregation (bulk CuO_x and/or CeO_2), which led to lower activity with $y \geq 0.75$. Similarly, Jabłońska et al. [10] and Wang et al. [24] reported poor ammonia conversion due to formation of bulk CuO and/or CeO_2, respectively. For Ga-modified samples, firstly the reduction temperatures increased for $y \leq 0.25$ (from 310 to 317 °C), then subsequently decreased to 312 °C, and afterwards increased with increasing Ga-loading (323 °C for $y = 1$). Again, $Ga_{0.25}$–Cu–Mg–Al–O_x presented a sharp H_2-TPR profile that turned to more bulky for higher gallium loadings. The dispersion of copper oxide species changed over $y \geq 0.5$, together with the distribution of ammonia products. Hence, $Ga_{0.25}$–Cu–Mg–Al–O_x showed higher selectivity to N_2 than $Ga_{0.5}$–Cu–Mg–Al–O_x. The profile for Ga_1–Cu–Mg–Al–O_x showed the highest reduction temperature. This result reflected the formation of bulk CuO_x, which are characterized by lower reducibility [7,13].

Concluding, Ga-modified catalysts (up to 0.25) reached a lower reduction temperature ($y = 0.25$, 317 °C) than Ag, or Ce-related samples ($y = 0.25$, 330 or 319 °C, respectively). Thus, the presence of gallium resulted in a significant increase in CuO_x dispersion compared to other incorporated metals. The order of the catalytic activity in the ammonia oxidation stayed as follows: $Ga_{0.25} \rightarrow Ce_{0.25} \rightarrow Ag_{0.25}$–Cu–Mg–Al–$O_x$. The selectivity to N_2 depended on the amount of easily reducible CuO_x, thus, the highest selectivity reached $Ag_{0.25}$, followed by $Ga_{0.25}$, and finally $Ce_{0.25}$–Cu–Mg–Al–O_x (based on H_2-TPR profiles intensity; H_2 uptake). The textural properties did not significantly influence

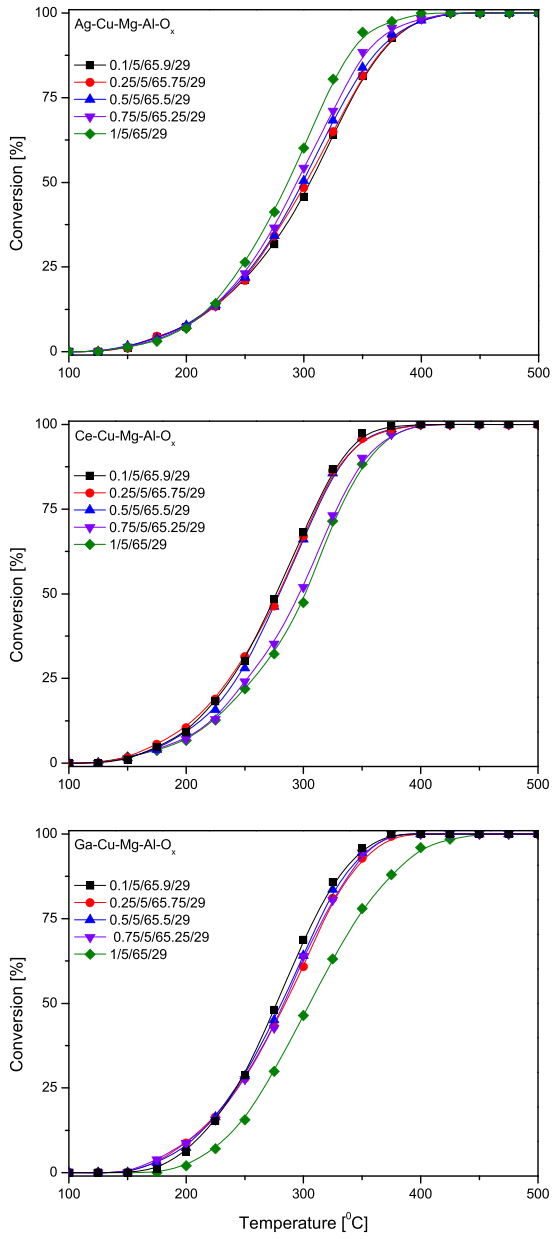

Fig. 8. Comparison of the results of catalytic activity for NH_3-SCO performed over mixed metal oxides. Experimental conditions: mass of catalysts = 100 mg, $[NH_3] = 0.5\%$, $[O_2] = 2.5\%$, [Ar] = 97%, total flow rate = 40 cm^3/min, WHSV = 24,000 cm^3/h g, linear heating of 5 K/min.

the catalytic performance of all tested mixed metal oxides. Ce- or Ga-containing catalysts revealed higher specific surface areas, higher amount of chemisorbed ammonia and acid density than corresponding Ag-containing catalysts. However, the presence of mesopores in mixed metal oxides could enable faster transport of the reactants to active surface sites and reaction products in a reverse direction, resulting in their enhanced catalytic performances. Furthermore, finely dispersed metal oxide species in Ce–Cu–Mg–Al–O_x and Ga–Cu–Mg–Al–O_x favoured NH_3 adsorption and activation, yielding enhanced activity. Such correlations were not found for Ag–Cu–Mg–Al–O_x. Thus, the order of catalytic performance followed the order obtained by H_2-TPR analysis. Taking into account materials with $y \geq 0.5$, the catalytic performance depended on the existing bulk phases rather than the reducibility of CuO_x. For instance, Ce–Cu–Mg–Al–O_x ($y \geq 0.75$) reached the lowest reduction temperature while the activity for these two materials significantly dropped compared to the other Ce-containing catalysts. In addition, the catalytic performances for Ag- and Ga-rich samples varied depending on the amount of the bulk phases. Future studies will certainly aim for a deeper understanding of the contribution of oxidative-reductive properties to catalytic activity.

4. Conclusions

We successfully synthesized Ag(Ce, Ga)–Cu–Mg–Al hydrotalcite-like compounds with intended molar ratios of (Ag(Ce, Ga):Cu:Mg:Al = y:5:66–y:29, y = 0–1). The thermal treatment led to the appearance of mixed metal oxides with a main structure of poorly crystallized MgO. Physicochemical characterization of as-synthesized hydrotalcite-like compounds and their derivatives revealed a successful incorporation of the additional metals for $y \leq 0.25$. The higher loading possibly led to formation of surface and bulk copper oxide species as well as aggregation of other phases. We found a correlation between H_2-TPR and NH_3-SCO for Ag(Ce, Ga)–Cu–Mg–Al hydrotalcite derived mixed metal oxides with $y \leq 0.25$ of metal loading. Thus, the easily reducible CuO_x led to high activity and a decreased selectivity to N_2 at higher temperatures. At higher metal loading ($y \geq 0.5$), the catalytic performance depended on bulk and surface segregated phases. We selected $Ga_{0.25}$–Cu–Mg–Al–O_x and $Ag_{0.25}$–Cu–Mg–Al–O_x as promising catalysts for selective ammonia oxidation. Further optimization of both catalysts based on the presented structure–activity relations is underway under conditions as present in real diesel car exhaust systems.

Acknowledgement

Funded by the Excellence Initiative of the German federal and state governments in the frame of the Center for Automotive Catalytic Systems Aachen (ACA) at RWTH Aachen University.

Appendix A. Supplementary data

Supplementary data associated with this article can be found, in the online version, at http://dx.doi.org/10.1016/j.apcatb.2017.01.079.

References

[1] F. Cavani, F. Trifirò, A. Vaccari, Hydrotalcite-type anionic clays: preparation, properties and applications, Catal. Today 11 (1991) 173–301.
[2] A. Vaccari, Preparation and catalytic properties of cationic and anionic clays, Catal. Today 41 (1998) 53–71.
[3] M. Nayak, T.R.N. Kutty, V. Jayaraman, G. Periaswamy, Preparation of the layered double hydroxide (LDH) LiAl2(OH)$_7$.2H$_2$O, by gel to crystallite conversion and a hydrothermal method, and its conversion to lithium aluminates, J. Mater. Chem. 7 (1997) 2131–2137.
[4] A. Besserguenev, A. Fogg, R. Francis, S. Price, D. O'hare, V. Isupov, B. Tolochko, Synthesis and structure of the gibbsite intercalation compounds [LiAl$_2$(OH)$_6$] X {X = Cl, Br, NO$_3$} and [LiAl$_2$(OH)$_6$]Cl.H$_2$O using synchrotron X-ray and neutron powder diffraction, Chem. Mater. 9 (1997) 241–247.
[5] O. Saber, Preparation and characterization of a new nano layered material, Co–Zr LDH, J. Mater. Sci. 42 (2007) 9905–9912.
[6] D. Tichit, N. Das, B. Coq, R. Durand, Preparation of Zr-containing layered double hydroxides and characterization of the acido-basic properties of their mixed oxides, Chem. Mater. 14 (2002) 1530–1538.
[7] L. Chmielarz, A. Węgrzyn, M. Wojciechowska, S. Witkowski, M. Michalik, Selective catalytic oxidation (SCO) of ammonia to nitrogen over hydrotalcite originated Mg–Cu–Fe mixed metal oxides, Catal. Lett. 141 (2011) 1345–1354.
[8] M. Jabłońska, L. Chmielarz, A. Węgrzyn, S. Witkowski, M. Michalik, Mixed metal oxides Mg–Cu–Fe obtained from hydrotalcites as catalysts for selective oxidation of ammonia to nitrogen and water vapor (SCO), CHEMIK 66 (2012) 750–757.
[9] M. Jabłońska, R. Palkovits, Copper based catalysts for the selective ammonia oxidation into nitrogen and water vapour—recent trends and open challenges, Appl. Catal. B: Environ. 181 (2016) 332–351.

[10] M. Jabłońska, M. Nocuń, K. Gołąbek, R. Palkovits, Effect of preparation procedures on catalytic activity of copper-based mixed oxides in selective catalytic oxidation of ammonia into nitrogen and water vapour. Submitted.
[11] L. Chmielarz, M. Jabłońska, A. Strumiński, Z. Piwowarska, A. Węgrzyn, S. Witkowski, M. Michalik, Selective catalytic oxidation of ammonia to nitrogen over Mg–Al, Cu–Mg–Al and Fe–Mg–Al mixed metal oxides doped with noble metals, Appl. Catal. B: Environ. 130 (2013) 152–162.
[12] M. Jabłońska, TPR study and catalytic performance of noble metals modified Al_2O_3, TiO_2 and ZrO_2 for low-temperature NH_3-SCO, Catal. Commun. 70 (2015) 66–71.
[13] M. Jabłońska, L. Chmielarz, A. Węgrzyn, K. Guzik, Z. Piwowarska, S. Witkowski, R.I. Walton, P.W. Dunne, F. Kovanda, Thermal transformations of Cu–Mg (Zn)–Al (Fe) hydrotalcite-like materials into metal oxide systems and their catalytic activity in selective oxidation of ammonia to dinitrogen, J. Thermal Anal. Calorim. 114 (2013) 731–747.
[14] Z. Wang, L. Wang, F. He, Z. Jiang, T. Xiao, Z. Zhang, Catalytic soot oxidation over Ce-and Cu-doped hydrotalcites-derived mesoporous mixed oxides, J Nanosci. Nanotechnol. 14 (2014) 7087–7096.
[15] J. Xu, H. Yue, S. Liu, H. Wang, Y. Du, C. Xu, W. Dong, C. Liu, Cu-Ag/hydrotalcite catalysts for dehydrogenative cross-coupling of primary and secondary benzylic alcohols, RSC Adv. 6 (2016) 24164–24174.
[16] X. Zheng, Q. Zhang, Y. Guo, W. Zhan, Y. Guo, Y. Wang, G. Lu, Epoxidation of propylene by molecular oxygen over supported Ag–Cu bimetallic catalysts with low Ag loading, J. Mol. Catal. A: Chem. 357 (2012) 106–111.
[17] Y. Huang, H. Ariga, X. Zheng, X. Duan, S. Takakusagi, K. Asakura, Y. Yuan, Silver-modulated SiO_2-supported copper catalysts for selective hydrogenation of dimethyl oxalate to ethylene glycol, J. Catal. 307 (2013) 74–83.
[18] M. Jabłońska, M. Nocuń, E. Bidzińska, Silver–alumina catalysts for low-temperature methanol incineration, Catal. Lett. 146 (2016) 937–944.
[19] D. Sun, Y. Yamada, S. Sato, Effect of Ag loading on Cu/Al_2O_3 catalyst in the production of 1,2-propanediol from glycerol, Appl. Catal. A: Gen. 475 (2014) 63–68.
[20] Z. Wang, L. Wang, F. He, Z. Jiang, T. Xiao, Z. Zhang, Catalytic soot oxidation over Ce- and Cu-doped hydrotalcites-derived mesoporous mixed oxides, J. Nanosci. Nanotechnol. 14 (2014) 7087–7096.
[21] B. Wen, M. He, Study of the Cu–Ce synergism for NO reduction with CO in the presence of O_2, H_2O and SO_2 in FCC operation, Appl. Catal. B: Environ. 37 (2002) 75–82.
[22] M. Crivello, C. Pérez, E. Herrero, G. Ghione, S. Casuscelli, E. Rodríguez-Castellón, Characterization of Al–Cu and Al–Cu–Mg mixed oxides and their catalytic activity in dehydrogenation of 2-octanol, Catal. Today 107 (2005) 215–222.
[23] L. Chmielarz, M. Rutkowska, P. Kuśtrowski, M. Drozdek, Z. Piwowarska, B. Dudek, R. Dziembaj, M. Michalik, An influence of thermal treatment conditions of hydrotalcite-like materials on their catalytic activity in the process of N_2O decomposition, J. Thermal Anal. Calorim. 105 (2011) 161–170.
[24] Z. Wang, Z. Qu, X. Quan, Z. Li, H. Wang, R. Fan, Selective catalytic oxidation of ammonia to nitrogen over $CuO–CeO_2$ mixed oxides prepared by surfactant-templated method, Appl. Catal. B: Environ. 134–135 (2013) 153–166.
[25] E. Angelescu, O. Pavel, R. Birjega, M. Florea, R. Zăvoianu, The impact of the "memory effect" on the catalytic activity of Mg/Al; Mg, Zn/Al; Mg/Al, Ga hydrotalcite-like compounds used as catalysts for cycloxene epoxidation, Appl. Catal. A: Gen. 341 (2008) 50–57.
[26] G.S. Macala, A.W. Robertson, C.L. Johnson, Z.B. Day, R.S. Lewis, M.G. White, A.V. Iretskii, P.C. Ford, Transesterification catalysts from iron doped hydrotalcite-like precursors: solid bases for biodiesel production, Catal. Lett. 122 (2008) 205–209.
[27] P. Sun, G. Siddiqi, M. Chi, A.T. Bell, Synthesis and characterization of a new catalyst Pt/Mg (Ga)(Al) O for alkane dehydrogenation, J. Catal. 274 (2010) 192–199.
[28] V.R. Choudhary, S.K. Jana, V.S. Narkhede, Benzylation and benzoylation of substituted benzenes over solid catalysts containing Ga- and Mg-oxides and/or chlorides derived from Ga–Mg-hydrotalcite by its HCl pre-treatment or calcination, Appl. Catal. A: Gen. 235 (2002) 207–215.
[29] A. Venugopal, J. Palgunadi, J.K. Deog, O.-S. Joo, C.-H. Shin, Dimethyl ether synthesis on the admixed catalysts of Cu–Zn–Al–M (M = Ga, La, Y, Zr) and γ-Al_2O_3: the role of modifier, J. Mol. Catal. A: Chem. 302 (2009) 20–27.
[30] G.L. Castiglioni, M. Ferrari, A. Guercio, A. Vaccari, R. Lancia, C. Fumagalli, Chromium-free catalysts for selective vapor phase hydrogenation of maleic anhydride to γ-butyrolactone, Catal. Today 27 (1996) 181–186.
[31] A. Bienholz, R. Blume, A. Knop-Gericke, F. Girgsdies, M. Behrens, P. Claus, Prevention of catalyst deactivation in the hydrogenolysis of glycerol by Ga_2O_3-modified copper/zinc oxide catalysts, J. Phys. Chem. C 115 (2010) 999–1005.
[32] P.B. Sanguineti, M.A. Baltanás, A.L. Bonivardi, Copper–gallia interaction in $Cu–Ga_2O_3–ZrO_2$ catalysts for methanol production from carbon oxide(s) hydrogenation, Appl. Catal. A: Gen. 504 (2015) 476–481.
[33] K. Faungnawakij, N. Shimoda, T. Fukunaga, R. Kikuchi, K. Eguchi, Cu-based spinel catalysts CuB_2O_4 (B = Fe, Mn, Cr, Ga, Al, $Fe_{0.75}$ $Mn_{0.25}$) for steam reforming of dimethyl ether, Appl. Catal. A: Gen. 341 (2008) 139–145.
[34] S.P. Newman, W. Jones, P. O'Connor, D.N. Stamires, Synthesis of the 3R2 polytype of a hydrotalcite-like mineral, J. Mater. Chem. 12 (2002) 153–155.
[35] X. Xu, L. Jiang, Z. Lü, J. Song, Z. Li, Influence of the pore structure of Ce/MgAl hydrotalcite-derived mixed oxides on its SO_x pick-up capacity, Chin. Sci. Bull. 58 (2013) 1670–1674.
[36] R.t. Shannon, Revised effective ionic radii and systematic studies of interatomic distances in halides and chalcogenides, Acta Crystallogr. Sect. A: Cryst. Phys. Diffract. Theor. Gen. Crystallogr. 32 (1976) 751–767.
[37] A.L. Allred, E.G. Rochow, A scale of electronegativity based on electrostatic force, J. Inorg. Nucl. Chem. 5 (1958) 264–268.
[38] J.S. Valente, J. Hernandez-Cortez, M.S. Cantu, G. Ferrat, E. López-Salinas, Calcined layered double hydroxides Mg–Me–Al (Me: Cu, Fe, Ni, Zn) as bifunctional catalysts, Catal. Today 150 (2010) 340–345.
[39] S. Velu, K. Suzuki, T. Osaki, F. Ohashi, S. Tomura, Synthesis of new Sn incorporated layered double hydroxides and their evolution to mixed oxides, Mater. Res. Bull. 34 (1999) 1707–1717.
[40] S. Velu, N. Shah, T. Jyothi, S. Sivasanker, Effect of manganese substitution on the physicochemical properties and catalytic toluene oxidation activities of Mg–Al layered double hydroxides, Micropor. Mesopor. Mater. 33 (1999) 61–75.
[41] M. Sanchez-Cantu, L.M. Perez-Diaz, A.M. Maubert, J.S. Valente, Dependence of chemical composition of calcined hydrotalcite-like compounds for SO_x reduction, Catal. Today 150 (2010) 332–339.
[42] M. Jabłońska, L. Chmielarz, A. Węgrzyn, K. Góra-Marek, Z. Piwowarska, S. Witkowski, E. Bidzińska, P. Kuśtrowski, A. Wach, D. Majda, Hydrotalcite derived (Cu, Mn)–Mg–Al metal oxide systems doped with palladium as catalysts for low-temperature methanol incineration, Appl. Clay Sci. 114 (2015) 273–282.
[43] J. Das, D. Das, K.M. Parida, Preparation and characterization of Mg–Al hydrotalcite-like compounds containing cerium, J. Colloid Interf. Sci. 301 (2006) 569–574.
[44] P. Sun, G. Siddiqi, M. Chi, A.T. Bell, Synthesis and characterization of a new catalyst Pt/Mg(Ga)(Al)O for alkane dehydrogenation, J. Catal. 274 (2010) 192–199.
[45] A. Pérez, M. Montes, R. Molina, S. Moreno, Cooperative effect of Ce and Pr in the catalytic combustion of ethanol in mixed Cu/CoMgAl oxides obtained from hydrotalcites, Appl. Catal. A: Gen. 408 (2011) 96–104.
[46] T.J. Vulic, A.F. Reitzmann, K. Lázár, Thermally activated iron containing layered double hydroxides as potential catalyst for N_2O abatement, Chem. Eng. J. 207 (2012) 913–922.
[47] S. Abelló, J. Pérez-Ramírez, Steam activation of Mg–Al hydrotalcite. Influence on the properties of the derived mixed oxides, Micropor. Mesopor. Mater. 96 (2006) 102–108.
[48] F. Prinetto, G. Ghiotti, P. Graffin, D. Tichit, Synthesis and characterization of sol–gel Mg/Al and Ni/Al layered double hydroxides and comparison with co-precipitated samples, Micropor. Mesopor. Mater. 39 (2000) 229–247.
[49] L. Chmielarz, P. Kuśtrowski, A. Rafalska-Łasocha, R. Dziembaj, Selective oxidation of ammonia to nitrogen on transition metal containing mixed metal oxides, Appl. Catal. B: Environ. 58 (2005) 235–244.
[50] K. Narasimharao, E. Al-Sabban, T.S. Saleh, A.G. Gallastegui, A.C. Sanfiz, S. Basahel, S. Al-Thabaiti, A. Alyoubi, A. Obaid, M. Mokhtar, Microwave assisted efficient protocol for the classic Ullmann homocoupling reaction using Cu–Mg–Al hydrotalcite catalysts, J. Mol. Catal. A: Chem. 379 (2013) 152–162.
[51] R. Ladera, F.J. Pérez-Alonso, J.M. González-Carballo, M. Ojeda, S. Rojas, J.L.G. Fierro, Catalytic valorization of CO_2 via methanol synthesis with Ga-promoted $Cu–ZnO–ZrO_2$ catalysts, Appl. Catal. B: Environ. 142–143 (2013) 241–248.
[52] V. Santos, M. Pereira, J. Órfão, J. Figueiredo, The role of lattice oxygen on the activity of manganese oxides towards the oxidation of volatile organic compounds, Appl. Catal. B: Environ. 99 (2010) 353–363.
[53] W. Shan, Z. Feng, Z. Li, J. Zhang, W. Shen, C. Li, Oxidative steam reforming of methanol on $Ce_{0.9}Cu_{0.1}OY$ catalysts prepared by deposition–precipitation, coprecipitation, and complexation–combustion methods, J. Catal. 228 (2004) 206–217.
[54] P. Talukdar, B. Bhaduri, N. Verma, Catalytic oxidation of NO over CNF/ACF-supported CeO_2 and Cu nanoparticles at room temperature, Indus. Eng. Chem. Res. 53 (2014) 12537–12547.
[55] J.-C. Lou, C.-M. Hung, S.-F. Yang, Selective catalytic oxidation of ammonia over copper–cerium composite catalyst, J. Air Waste Manage. Assoc. 54 (2004) 68–76.
[56] C.-M. Hung, Selective catalytic oxidation of ammonia to nitrogen on $CuO–CeO_2$ bimetallic oxide catalysts, Aerosol Air Qual. Res. 6 (2006) 150–169.
[57] M. Jabłońska, TPR study and catalytic performance of noble metals modified Al_2O_3, TiO_2 and ZrO_2 for low-temperature NH_3-SCO, Catal. Commun. 70 (2015) 66–71.
[58] T. Curtin, S. Lenihan, Copper exchanged beta zeolites for the catalytic oxidation of ammonia, Chem. Commun. (2003) 1280–1281.
[59] M. Yang, C. Wu, C. Zhang, H. He, Selective oxidation of ammonia over copper–silver-based catalysts, Catal. Today 90 (2004) 263–267.